Liu Wang
Department of Aerospace Engineering and Engineering Mechanics,
Center for Mechanics of Solids, Structures and Materials,
The University of Texas at Austin,
Austin, TX 78712

Shutao Qiao
Department of Aerospace Engineering and Engineering Mechanics,
Center for Mechanics of Solids, Structures and Materials,
The University of Texas at Austin,
Austin, TX 78712

Shideh Kabiri Ameri
Department of Electrical and Computer Engineering,
The University of Texas at Austin,
Austin, TX 78712

Hyoyoung Jeong
Department of Electrical and Computer Engineering,
The University of Texas at Austin,
Austin, TX 78712

Nanshu Lu[1]
Department of Aerospace Engineering and Engineering Mechanics,
Center for Mechanics of Solids, Structures and Materials,
The University of Texas at Austin,
210 E. 24th Street,
Austin, TX 78712;
Department of Electrical and Computer Engineering,
The University of Texas at Austin,
Austin, TX 78712;
Department of Biomedical Engineering,
The University of Texas at Austin,
Austin, TX 78712;
Texas Materials Institute,
The University of Texas at Austin,
Austin, TX 78712
e-mail: nanshulu@utexas.edu

A Thin Elastic Membrane Conformed to a Soft and Rough Substrate Subjected to Stretching/Compression

Conformability of bio-integrated electronics to soft and microscopically rough biotissues can enhance effective electronics–tissue interface adhesion and can facilitate signal/heat/mass transfer across the interface. When biotissues deform, for example, when skin stretches or heart beats, the deformation may lead to changes in conformability. Although a theory concerning just full conformability (FC) under deformation has been developed (i.e., the FC theory), there is no available theory for partially conformable (PC) systems subjected to deformation. Taking advantage of the path-independent feature of elastic deformation, we find that the total energy of a PC system subjected to stretching or compression can be analytically expressed and minimized. We discover that the FC theory is not sufficient in predicting FC and a full energy landscape obtained by our PC theory is needed for searching for the equilibrium. Our results reveal that stretching enhances conformability while compression degrades it. In addition to predicting the critical parameters to maintain FC under deformation, our PC theory can also be applied to predict the critical compressive strain beyond which FC is lost. Our theory has been validated by laminating poly(methyl methacrylate) (PMMA) membranes of different thicknesses on human skin and inducing skin deformation. [DOI: 10.1115/1.4037740]

Keywords: bio-integrated electronics, bio-electronics interface, conformability, energy minimization

1 Introduction

In recent years, soft bio-integrated electronics have gathered growing attention due to their unlimited potential in disease monitoring, diagnosis, and treatment, as well as in human–machine interaction [1,2]. Tremendous efforts have been made to improve device flexibility and stretchability [3–5], materials [6–8], and processing [9–11], as well as functionalities and use cases [2,12–14]. In addition to extensive research on the devices, bio-electronics interface is also an interesting topic [15–18] because people have realized that intimate and secure contact between the thin film device and the bio-tissue is of great importance to the sensitivity and signal-to-noise ratio of both in vivo [19,20] and epidermal [12,21,22] devices.

Without losing generality, the thin film device has been effectively modeled as a thin elastic membrane, and the bio-tissue has been idealized as a semi-infinite soft substrate with a sinusoidal surface profile [15,17,18]. When a thin membrane is laminated on a soft and rough substrate, three contact modes are possible: (1) fully conformed (FC), i.e., the membrane forms full contact with the substrate without any interfacial gap; (2) partially conformed (PC), i.e., only some areas of the membrane contact with the substrate; and (3) nonconformed (NC), i.e., the membrane remains flat if gravity is neglected.

The method of energy minimization has been widely applied to determine the equilibrium membrane–substrate contact modes. The total energy of the system consists of bending energy of the membrane (membrane energy is omitted due to neglected membrane–substrate shear stress), elastic energy stored in the deformed substrate, and membrane–substrate interface adhesion energy. A major difficulty in this method is to determine the elastic energy stored in the substrate after it contacts with the

[1]Corresponding author.
Contributed by the Applied Mechanics Division of ASME for publication in the JOURNAL OF APPLIED MECHANICS. Manuscript received July 24, 2017; final manuscript received August 20, 2017; published online September 12, 2017. Editor: Yonggang Huang.

membrane. One idea to bypass it is to prescribe a known surface displacement for the substrate. For example, under FC condition, Wang et al. [15] assumed that the substrate deforms from its initially sinusoidal profile to another sinusoidal shape with the same wavelength but a different amplitude. As the corresponding surface traction to induce such displacement is easy to obtain, the elastic energy stored in the deformed substrate can be readily calculated as the work done by such surface traction. However, this FC theory is not able to predict the PC scenario. Therefore, we introduced a *partially conformed theory* where we assumed that within the PC zone, the substrate surface deforms from one sinusoidal shape to another with the same wavelength but a different amplitude [18]. This assumption legitimately originates from the FC theory and can recover the FC theory. After prescribing sinusoidal displacement in the PC zone, we have successfully obtained the corresponding traction within the PC zone and could therefore express the elastic energy stored in the deformed substrate [18].

However, equilibrium analysis between membrane and a relaxed substrate is not sufficient for bio-integrated electronics because in reality, biotissues are dynamic. The degree of conformability can be easily changed by the contraction and expansion of the biotissues. Therefore, being able to understand and to further control the quality of contact between the thin film device and the dynamic biotissue is of practical significance. The conformability of a thin elastic membrane laminated on a soft corrugated substrate subjected to stretching/compression has been analyzed using the FC theory [17,23]. First, the FC theory dismisses the possibility of the PC mode and the minimization of the total energy is implemented only within the FC and NC modes. As a result, the energy minimum found by the FC theory may not be the global minimum and the predicted critical conditions for FC may not be enough to reach actual FC. Second, in Refs. [17,23], the substrate energy U_s are miscalculated by adopting a positive sign in front of the applied strain ϵ_0 ($\epsilon_0 > 0$ for tension and $\epsilon_0 < 0$ for compression), which should have been a negative sign according to Refs. [24,25].

Because of these concerns, we would like to develop a PC theory for analyzing the conformability between a membrane and a soft and rough substrate when the system is subjected to lateral deformation. The difficulty is how to express substrate energy after lateral deformation. To do this, let us first consider the following two different loading paths for FC (Fig. 1) and PC (Fig. 2). In Figs. 1 and 2, state 0 is the initial state of the system in which the membrane is flat and does not contact with the substrate. Loading path (a) can be called the laminate-stretching path, which means that the membrane is first laminated on a relaxed substrate and the system reaches equilibrium (state 1, FC in Fig. 1(*a*) or PC in Fig. 2(*a*)); then, a lateral strain ϵ_0 is applied to both the substrate and the membrane and the system reaches another equilibrium (state 2, FC in Fig. 1(*a*) or PC in Fig. 2(*a*)). In contrast, loading path (b) illustrated in Fig. 1(*b*) can be called the stretch-laminating path. The difference in loading path (b) is that the external load ϵ_0 is applied first, FC in Fig. 1(*b*) or PC in Fig. 2(*b*)), and then, the membrane is brought into contact with the substrate and the system equilibrates (state 2, FC in Fig. 1(*b*) or PC in Fig. 2(*b*)).

In Sec. 2, we will first prove that the two loading paths are equivalent for FC in the sense that state 2 achieved by path (a) and path (b) are the same, i.e., with the same total energy (Fig. 1). Drawing an analogy to the PC case, we will obtain the total energy of state 2 through loading path (b) in Fig. 2. The different results obtained by the FC theory and the PC theory are compared in Sec. 3. Also in Sec. 3, we provided experimental validation to the PC theory by laminating poly(methyl methacrylate) (PMMA) membranes of different thicknesses on human skin and inducing skin deformation. Conclusion is offered in Sec. 4.

2 Theoretical Analysis

2.1 Fully Conformed Theory: Loading Path (a). For simplicity, the membrane is modeled as a uniform linear elastic membrane with plane strain modulus $\bar{E}_m$ and thickness t. The soft substrate is assumed to be a precorrugated linear elastic half space with plane strain modulus $\bar{E}_s$. Initially, i.e., at state 0 in Fig. 1, the surface profile of the undeformed substrate is simply characterized by a sinusoidal equation

$$w_0(x) = h_0\left(1 + \cos\frac{2\pi x}{\lambda_0}\right) \tag{1}$$

where h_0 and λ_0 denote the semi-amplitude and wavelength of the undeformed substrate surface, respectively. Both the membrane and the substrate are stress free in state 0.

2.1.1 State 1 in Loading Path (a). When the membrane is laminated on the soft substrate, it starts to conform to the substrate driven by the membrane–substrate interfacial adhesion. If FC is

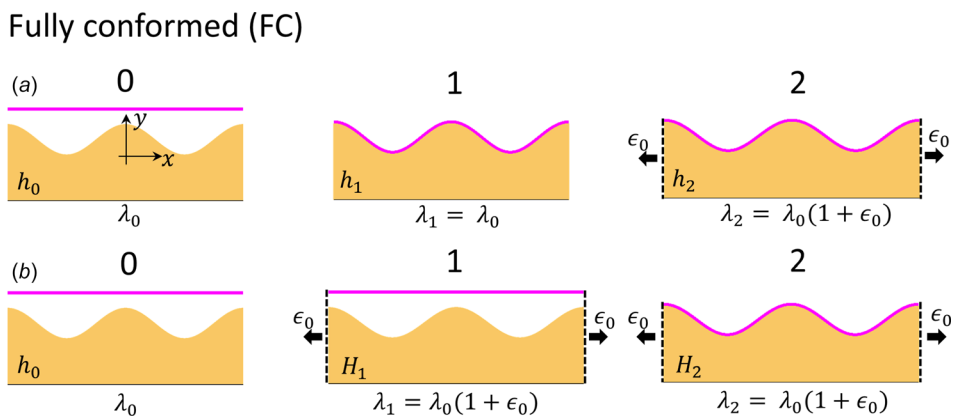

Fig. 1 Schematics of a thin elastic membrane fully conformed to a soft corrugated substrate following two different loading paths: (*a*) The laminate-stretching path: the membrane first laminates on the substrate and the system is then subjected to lateral strain ϵ_0. At equilibrium, the substrate surface is characterized by its semi-amplitude and wavelength, i.e., (h_0, λ_0) at state 0; (h_1, λ_1) at state 1; (h_2, λ_2) at state 2. (*b*) The stretch-laminating path: the membrane and substrate are first subjected to ϵ_0 and then laminated together with ϵ_0 still applied. At equilibrium, the substrate surface is characterized by (h_0, λ_0) at state 0; (H_1, λ_1) at state 1; (H_2, λ_2) at state 2.

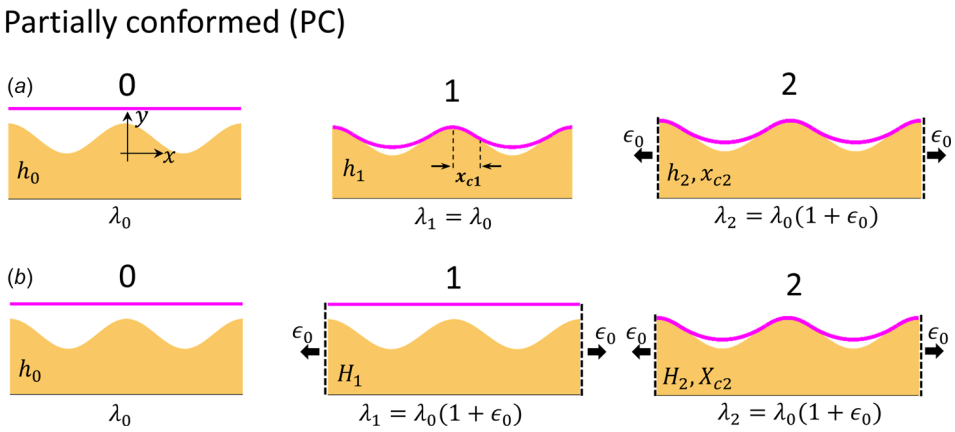

Fig. 2 Schematics of a thin elastic membrane partially conformed to a soft corrugated substrate following two different loading paths similar to Fig. 1. (*a*) The laminate-stretching path: at equilibrium, the substrate is characterized by (x_{c1}, h_1, λ_1) at state 1; (x_{c2}, h_2, λ_2) at state 2 where x_c reflects the contact zone size. (*b*) At equilibrium, the substrate is characterized by (H_1, λ_1) at state 1; (X_{c2}, H_2, λ_2) at state 2.

achieved, i.e., state 1 in Fig. 1(*a*), the profiles of both the substrate and the membrane are the same

$$w_1(x) = h_1\left(1+\cos\frac{2\pi x}{\lambda_1}\right) \tag{2}$$

where h_1 and λ_1 are the semi-amplitude and wavelength. Since no lateral deformation is applied in state 1 of Fig. 1(*a*), the wavelength remains unchanged, i.e., $\lambda_1 = \lambda_0$. In addition, since the interfacial shear stress can be neglected when the membrane is reasonably stiff [26], the membrane energy can neglected at state 1, i.e., $U_{\text{membrane}} \approx 0$. Hence, the total energy of the system at state 1 in Fig. 1(*a*), U_1^a, consists of the following three energies:

$$U_1^a = U_{b1}^a + U_{ad1}^a + U_{s1}^a \tag{3}$$

where superscript a represents loading path (a), subscript 1 denotes state 1, U_{b1}^a is the bending energy of the membrane, U_{ad1}^a is the interfacial adhesion energy between the membrane and the substrate, and U_{s1}^a is the elastic energy stored in the substrate. Bending energy and adhesion energy per wavelength can be readily written as

$$U_{b1} = \frac{1}{2\lambda_1}\int_0^{\lambda_1}\overline{E}_m I\kappa_1^2 dx \approx \frac{1}{2\lambda_1}\int_0^{\lambda_1}\overline{E}_m I\left(w_1''\right)^2 dx = \frac{4h_1^2\pi^4}{\lambda_1^4}\overline{E}_m I$$
$$U_{ad1} = -\frac{1}{\lambda_1}\int_0^{\lambda_1}\gamma ds \approx -\frac{\gamma}{\lambda_1}\int_0^{\lambda_1}\left[1+\frac{1}{2}\left(w_1'\right)^2\right]dx = -\gamma\left(1+\frac{\pi^2h_1^2}{\lambda_1^2}\right) \tag{4}$$

where $\overline{E}_m I = \overline{E}_m t^3/12$ is the plane strain bending stiffness of the membrane, $\kappa_1 \approx w_1''$ is its curvature assuming slight waviness, γ is the membrane-substrate work of adhesion, $ds \approx (1 + +1/2(w_1')^2)dx$ is an infinitesimal segment of the curve.

As for the substrate energy (U_{s1}^a), it should equal to the work done by the surface tractions on the substrate. The surface displacement of the substrate is given by $u(x) = w_1(x) - w_0(x)$, and the surface traction to induce such a surface displacement is found to be $p(x) = -\pi\overline{E}_s/\lambda_1(h_1 - h_0)\cos(2\pi x/\lambda_1)$ [25,26], which yields the following substrate energy per wavelength:

$$U_{s1}^a = \frac{1}{\lambda_1}\int_0^{\lambda_1}\frac{1}{2}u(x)p(x)dx = \overline{E}_s\frac{\pi}{4}\frac{(h_0-h_1)^2}{\lambda_1} \tag{5}$$

After introducing five nondimensional parameters $\alpha = \overline{E}_m/\overline{E}_s$, $\beta = 2\pi h_0/\lambda_0, \eta = t/\lambda_0, \mu = \gamma/\overline{E}_s\lambda_0$, and $\xi = h_1/h_0$, which are normalized membrane stiffness, substrate roughness, membrane thickness, work of adhesion, and substrate amplitude, respectively, the normalized total energy of the system in state 1 can be rewritten as

$$\widehat{U}_1^a = \frac{U_1^a}{\overline{E}_s\lambda_0\beta^2} = \frac{\pi^2}{12}\xi_1^2\alpha\eta^3 + \frac{1}{16\pi}(1-\xi_1)^2 - \mu\left(\frac{1}{\beta^2}+\frac{1}{4}\xi_1^2\right) \tag{6}$$

where $\widehat{U}_1^a$ is a function of five variables α, β, η, μ, and ξ_1. If α, β, η, and μ are given, minimization of $\widehat{U}_1^a$ with respect to ξ_1, i.e., $\partial\widehat{U}_1^a/\partial\xi_1 = 0$, gives the equilibrium state, which is achieved when

$$\xi_1 = \frac{h_1}{h_0} = \frac{3}{3+4\pi^3\alpha\eta^3 - 12\pi\mu} \tag{7}$$

The FC theory in Refs. [15,17] claims that the criterion for FC is that the total energy of the system at state 1 is lower than that of NC, i.e.,

$$\widehat{U}_1|_{\xi_1} < \widehat{U}_1|_{\text{NC}} = 0 \tag{8}$$

Solving the inequality in Eq. (8) yields

$$\alpha\eta^3 < \frac{3\left(4\mu+\beta^2\mu-16\pi\mu^2\right)}{\pi^2\left(\beta^2-16\pi\mu\right)} \tag{9}$$

When β and μ are given, Eq. (9) gives a condition that α and η should satisfy for FC. Results will be discussed in Sec. 3.

2.1.2 State 2 in Loading Path (a). Section 2.1.1 analyzed the contact between a thin elastic membrane and a relaxed soft substrate with wavy surface, i.e., state 1 in Fig. 1(*a*). After that, a lateral strain ϵ_0 is applied on both the substrate and the membrane, as illustrated by state 2 of Fig. 1(*a*). Assuming that the membrane still fully conforms to the substrate after the lateral strain is applied, the substrate will deform to state 2 with the following surface profile:

$$w_2(x) = h_2\left(1+\cos\frac{2\pi x}{\lambda_2}\right) \tag{10}$$

where the subscript 2 indicates the state 2, h_2 is the new semi-amplitude, and $\lambda_2 = \lambda_0(1+\epsilon_0)$ is the new wavelength.

Similarly, the bending energy of the membrane and the interfacial adhesion energy per wavelength at state 2 can be found as

$$U^a_{b2} = \frac{4h_2^2\pi^4}{\lambda_2^4}\overline{E}_m I$$
$$U^a_{ad2} = -\gamma\left(1 + \frac{\pi^2 h_2^2}{\lambda_2^2}\right) \tag{11}$$

while the substrate energy per wavelength becomes [24,25]

$$U^a_{s2} = \frac{\pi}{4\lambda_2}\overline{E}_s\left[(h_0 - h_2)^2 + 2h_0(h_2 - h_0)\epsilon_0\right] + C \tag{12}$$

The first term of Eq. (12) is the energy associated with the variation of the wavy surface while the second term C is a constant which is independent of h_2 (see the Appendix for the derivation of C). The membrane energy due to stretching is also a constant, i.e., $U^a_{m2} = \overline{E}_m t\epsilon_0^2/(2\lambda_2) \equiv D$. Since the total energy will be minimized by taking the variation with respect to h_2, the constant terms C and D can be dropped. Therefore, the normalized total energy at stage 2 of Fig. 1(*a*) is

$$\widehat{U}^a_2 = \frac{U^a_{t2}}{\overline{E}_s\lambda_2\beta'^2} = \frac{\pi^2}{12}\xi_2^2\alpha\eta'^3 + \frac{1}{16\pi}\left[(1-\xi_2)^2 + 2(\xi_2 - 1)\epsilon_0\right] - \mu'\left(\frac{1}{\beta'^2} + \frac{1}{4}\xi_2^2\right) \tag{13}$$

where $\beta' = \beta/(1+\epsilon_0), \eta' = \eta/(1+\epsilon_0), \mu' = \mu/(1+\epsilon_0)$ and $\xi_2 = h_2/h_0$.

Minimization of $\widehat{U}^a_2$ with respect to ξ_2, i.e., $\partial\widehat{U}^a_2/\partial\xi_2 = 0$, gives the equilibrium substrate semi-amplitude of state 2

$$\xi_2 = \frac{h_2}{h_0} = \frac{3(1-\epsilon_0)}{3 + 4\pi^3\alpha\eta'^3 - 12\pi\mu'} \tag{14}$$

Again, solving

$$\widehat{U}^a_2|_{\xi_2} < \widehat{U}^a_2|_{\text{NC}} = 0 \tag{15}$$

yields a new criterion for FC when lateral tension or compression is applied

$$\alpha\eta'^3 < \frac{3\left(4\mu' + \beta'^2\mu' - 16\pi\mu'^2\right)}{\pi^2\left(\beta'^2 - 16\pi\mu'\right)} \tag{16}$$

It is obvious that when $\epsilon_0 = 0$, Eqs. (14) and (16) will decay to Eqs. (7) and (9), respectively, which means state 2 will recover state 1 when there is no applied strain. This concludes the analysis of loading path (a) using the FC theory (Fig. 1(*a*)). Closed-form solutions have been obtained for both state 1 and state 2. Next, we need to obtain the solution to state 2 of loading path (b) (Fig. 1(*b*)) and prove that it is the same as state 2 of Fig. 1(*a*).

2.2 Fully Conformed Theory: Loading Path (b). In Fig. 1(*b*), the membrane and substrate are first stretched to state 1, and then the membrane is laminated to the substrate to achieve FC in state 2. We will use this loading path to find the solution to state 2.

2.2.1 State 1 in Loading Path (b). In Fig. 1(*b*) state 1, the membrane and the substrate are not in contact, and they are individually stretched. Therefore, the top surface of the corrugated substrate is traction free, in which case the wavelength of the substrate surface profile becomes $\lambda_1 = \lambda_0(1+\epsilon_0)$ and the semi-amplitude will simply change to $H_1 = h_0(1-\epsilon_0)$ under small ϵ_0 [25]. It is also obvious that both the bending energy of the membrane and the adhesion energy at state 1 are zero, i.e., $U^b_{b1} = U^b_{ad1} = 0$, where superscript b stands for loading path (b). The membrane energy due to stretching equals $U^b_{m1} = \overline{E}_m t\epsilon_0^2/(2\lambda_1) \equiv D$. Also, the substrate energy and membrane energy are found to be a constant $U^b_{s1} = C$, which is the same as the constant term C in Eq. (12) (see the Appendix for derivation).

2.2.2 State 2 in Loading Path (b). After each being stretched by ϵ_0 (state 1), the membrane is brought into contact with the substrate with ϵ_0 still applied on both. Assuming FC is achieved at equilibrium, as drawn in state 2 in Fig. 1(*b*), the semi-amplitude becomes H_2 while the wavelength remains to be $\lambda_2 = \lambda_0(1+\epsilon_0)$. The bending energy of the membrane and the adhesion energy can be written as

$$U^b_{b2} = \frac{4H_2^2\pi^4}{\lambda_2^4}\overline{E}_m I$$
$$U^b_{ad2} = -\gamma\left(1 + \frac{\pi^2 H_2^2}{\lambda_2^2}\right) \tag{17}$$

Considering the substrate energy at state 1, U^b_{s1} is a constant independent of the amplitude of the wavy surface, the deformation from state 1 to state 2 in loading path (b) is analogous to that from state 0 to state 1 in loading path (a), i.e., the membrane spontaneously conforms to a traction-free surface. As a result, we can calculate the substrate energy at state 2 by simply modifying Eq. (5)

$$U^b_{s2} = \frac{\pi}{4\lambda_2}\overline{E}_s(H_1 - H_2)^2 = \frac{\pi}{4\lambda_2}\overline{E}_s\left[(H_2 - h_0)^2 + 2h_0(H_2 - h_0)\epsilon_0\right] + O\left(\epsilon_0^2\right) \tag{18}$$

Since the stress–strain fields are calculated by linear perturbation method [25], higher order terms are omitted. Therefore, minimization of the total energy $\partial U^b_2/\partial H_2 = 0$ yields

$$\frac{H_2}{h_0} = \frac{3(1-\epsilon_0)}{3 + 4\pi^3\alpha\eta'^3 - 12\pi\mu'} \tag{19}$$

Comparing Eq. (19) with Eq. (14), we can see that $H_2 = h_2$, which proves that the two loading paths are completely equivalent. This is because stretching in state 1 of loading path (b) simply changes the surface profile of the substrate before it contacts the membrane without introducing nonconstant energy terms. Therefore, path (b) shows a potential for developing and solving the PC theory.

2.3 Partially Conformed Theory: Loading Path (a). In Secs. 2.1 and 2.2, we have proved that the laminate-stretching path and the stretch-laminating path can lead to the same final FC configuration. In this section, we will extend our model to the PC scenario.

2.3.1 State 1 in Loading Path (a). When a membrane is partially conformed to a corrugated substrate, as depicted by state 1 in Fig. 2(*a*), the contact zone is labeled to be $0 \le x \le x_{c1}$ while the detached zone is $x_{c1} \le x \le \lambda_1/2$. This PC state has been investigated in our pervious paper [18]. In the paper, we postulated that in PC mode, the substrate within the contact zone deforms from its initial sinusoidal profile to a new sinusoidal shape and within the detached zone $(x_{c1} \le x \le \lambda_0/2)$, the membrane simply takes a parabolic shape if the membrane stress is neglected and it is therefore under pure bending. Thus, the associated energies at state 1 can be calculated as

$$U^a_{b1} = \frac{4\pi^2 h_1^2\overline{E}_m I}{\lambda_1^4}D(\widehat{x}_{c1})$$
$$U^a_{ad1} = -\gamma E(\widehat{x}_{c1}, \xi_1, \beta) \tag{20}$$
$$U^a_{s1} = \frac{\overline{E}_s\lambda_1\beta^2(1-\xi_1)^2}{4\pi}F(\widehat{x}_{c1})$$

where $\lambda_1 = \lambda_0$, $\beta = 2\pi h_0/\lambda_0$, $\widehat{x}_{c1} = 2x_{c1}/\lambda_0$, $\xi_1 = h_1/h_0$, and

$$D(\hat{x}_{c1}) = \frac{2}{1-\hat{x}_{c1}}\sin^2(\pi\hat{x}_{c1}) + \pi^2\hat{x}_{c1} + \frac{\pi}{2}\sin(2\pi\hat{x}_{c1})$$
$$E(\hat{x}_{c1},\xi_1\beta) = \hat{x}_{c1}\left(1+\frac{(\xi_1\beta)^2}{4}\right) - \frac{(\xi_1\beta)^2}{8\pi}\sin(2\pi\hat{x}_{c1}) \quad (21)$$
$$F(\hat{x}_{c1}) = \frac{1}{4}\sin^4\left(\frac{\pi\hat{x}_{c1}}{2}\right)$$

When $\hat{x}_{c1}=1$, Eq. (20) decays to Eqs. (4) and (5) suggesting that our PC theory can successfully recover the FC theory when there is no detached zone. Note that, $F(\hat{x}_{c1})$ was numerically evaluated in Ref. [18] while we now have a way to analytically solve it (see the Appendix).

After introducing the contact zone variable $\hat{x}_{c1}$, the total energy of the system at state 1 becomes a function of six variables $\beta, \alpha, \eta, \mu, \xi_1$, and $\hat{x}_{c1}$

$$\hat{U}_1^a = \frac{U_1^a}{\bar{E}_s\lambda_0\beta^2} = \frac{\pi^2}{12}\xi_1^2\alpha\eta^3 D(\hat{x}_{c1}) - \frac{\mu}{\beta^2}E(\hat{x}_{c1},\xi_1\beta) + \frac{(1-\xi_1)^2}{4\pi}F(\hat{x}_{c1}) \quad (22)$$

When β, α, η, and μ are specified, minimization of $\hat{U}_1^a$ with respect to ξ_1 and $\hat{x}_{c1}$ will yield the equilibrium state. It is worth noting that at equilibrium, $\partial\hat{U}_1^a/\partial\hat{x}_{c1}=0$ is not always satisfied due to the fact that $\hat{x}_{c1}$ is limited within $0\le\hat{x}_{c1}\le 1$. But the condition $\partial\hat{U}_1^a/\partial\xi_1=0$ can always be met, which yields

$$\xi_1 = 3(1-\hat{x}_c)\sin^4\left(\frac{\pi\hat{x}_{c1}}{2}\right)\Big/\Big\{3(\hat{x}_{c1}-1)\sin^4\left(\frac{\pi\hat{x}_{c1}}{2}\right) + 2\Big[-4\pi\alpha\eta^3\sin^2(\pi\hat{x}_{c1}) + (\hat{x}_{c1}-1)\big(2\pi\hat{x}_{c1}(\pi^2\alpha\eta^3-3\mu) + (\pi^2\alpha\eta^3+3\mu)\sin(2\pi\hat{x}_{c1})\big)\Big]\Big\} \quad (23)$$

Plugging Eq. (23) into Eq. (22) simplifies the normalized total energy to have only five variables

$$\hat{U}_1^a(\alpha,\beta,\eta,\mu,\hat{x}_{c1}) \quad (24)$$

For the sake of space, the complete form of Eq. (24) is not provided here. For given β, α, η, and μ, normalized total energy $\hat{U}_1^a$ can be plotted as a function of $\hat{x}_{c1}$ in which minimal energy state can be found. The difference between conformability predicted by the FC theory, i.e., by the minimization of Eq. (6), and by the PC theory, i.e., by the minimization of Eq. (24), will be discussed in Sec. 3.

2.3.2 State 2 in Loading Path (a). State 1 in Fig. 2(*a*) has been analytically solved by the PC theory. However, after stretching or compression is applied, i.e., at state 2 in path (a), no analysis regarding the substrate energy is available to the best of our knowledge. Fortunately, we have shown that for the FC case, the two loading paths are interchangeable. Here, we presume that for the PC scenario, the two loading paths can still give identical results according to the following three arguments:

(1) Only small stretching/compression and slightly wavy surface are considered in this paper, i.e., $\epsilon_0 \ll 1$, $h_0/\lambda_0 \ll 1$. These are necessary conditions to derive explicit stress–strain fields by linear perturbation method in Refs. [24,25].
(2) Substrate deformation in PC mode is smaller than that of FC mode.
(3) PC theory can successfully recover the FC theory.

Herein, we assume that state 2 in the PC scenario can be analyzed by following path (b) in Fig. 2 in which the substrate is stretched first to have wavelength $\lambda_1=\lambda_0(1+\epsilon_0)$ and semi-amplitude $H_1=h_0(1-\epsilon_0)$ at state 1.

Therefore, by modifying Eq. (22), the normalized total energy at state 2 can be written as

$$\hat{U}_2^b = \frac{U_2^b}{\bar{E}_s\lambda_2\beta'^2} = \frac{\pi^2}{12}\xi_2^2\alpha\eta'^3 D(\hat{x}_{c2}) - \frac{\mu'}{\beta'^2}E(\hat{x}_{c2},\xi_2\beta') + \frac{(1-\epsilon_0-\xi_2)^2}{4\pi}F(\hat{x}_{c2}) \quad (25)$$

where $\beta'=\beta/(1+\epsilon_0)$, $\eta'=\eta/(1+\epsilon_0)$, $\mu'=\mu/(1+\epsilon_0)$, $\hat{x}_{c2}=2x_{c2}/\lambda_2$, $\xi_2=H_2/h_0$, and

$$D(\hat{x}_{c2}) = \frac{2}{1-\hat{x}_{c2}}\sin^2(\pi\hat{x}_{c2}) + \pi^2\hat{x}_{c2} + \frac{\pi}{2}\sin(2\pi\hat{x}_{c2})$$
$$E(\hat{x}_{c2},\xi_2\beta') = \hat{x}_{c2}\left(1+\frac{(\xi_2\beta')^2}{4}\right) - \frac{(\xi_2\beta')^2}{8\pi}\sin(2\pi\hat{x}_{c2}) \quad (26)$$
$$F(\hat{x}_{c2}) = \frac{1}{4}\sin^4\left(\frac{\pi\hat{x}_{c2}}{2}\right)$$

Similar analysis can be performed to obtain the equilibrium solution. The criterion to maintain FC when ϵ_0 is applied using the PC theory can be expressed as

$$\alpha\eta'^3 < f(\beta',\mu',\epsilon_0) \quad (27)$$

where $f(\beta',\mu',\epsilon_0)$ is numerically obtained. Results will be presented and discussed in Sec. 3.

3 Results

The criteria for a thin elastic membrane to fully conform to a soft corrugated substrate subjected to stretching/compression (state 2) have been obtained by the FC theory, i.e., Eq. (16), and by the PC theory, i.e., Eq. (27), respectively. Note that setting $\epsilon_0=0$ in Eqs. (16) and (27) will lead to the criterion for FC mode at state 1 in the FC and PC theory, respectively. By fixing the moduli of the substrate and membrane, the roughness of the substrate surface, and the interfacial work of adhesion, i.e., by fixing α, β, and μ, we can investigate the effect of membrane thickness, i.e., η, on the conformability. In this section, we will use the following numerical example to illustrate the idea. Considering a silicone membrane of $\bar{E}_m\approx 2$ MPa [23] laminating on human skin whose $h_0\approx 20$ μm, $\lambda_0\approx 150$ μm [27], and $\bar{E}_s\approx 130$ kPa [28]. The silicone–skin interface adhesion has been measured to be $\gamma\approx 0.21$ N/m [29]. Accordingly, the nondimensional parameters can be calculated as $\alpha=\bar{E}_m/\bar{E}_s=15.4$, $\beta=2\pi h_0/\lambda_0=0.8$, and $\mu=\gamma/(\bar{E}_s\lambda_0)=0.011$.

3.1 Laminating on Relaxed Substrate. On the one hand, plugging $\alpha=15.4, \beta=0.8, \mu=0.011$, and $\epsilon_0=0$ into Eq. (16) yields that the critical thickness of the membrane to fully conform to the skin is 31.5 μm, i.e., $\eta=0.21$. In other words, according to the FC theory, as long as the membrane is thinner than 31.5 μm, it will fully conform to a relaxed skin. On the other hand, according to the PC theory, the total energy at state 1 of loading path (a), $\hat{U}_1^a$ can be plotted as a function of the contact zone variable $\hat{x}_{c1}$. $\hat{U}_1^a$ versus $\hat{x}_{c1}$ curves with $\eta=0.11, 0.12, 0.13, 0.14, 0.15$, and 0.21 are plotted in Fig. 3(*a*). The three curves corresponding to $\eta=0.11, 0.12$ and 0.13 (red, blue, and black) all reach the global minimum at $\hat{x}_{c1}=1$, which indicates that the FC mode is energetically favorable. The difference is that for $\eta=0.11$ (red), $\hat{U}_1^a$ monotonically decreases with $\hat{x}_{c1}$, while for $\eta=0.12$ and 0.13

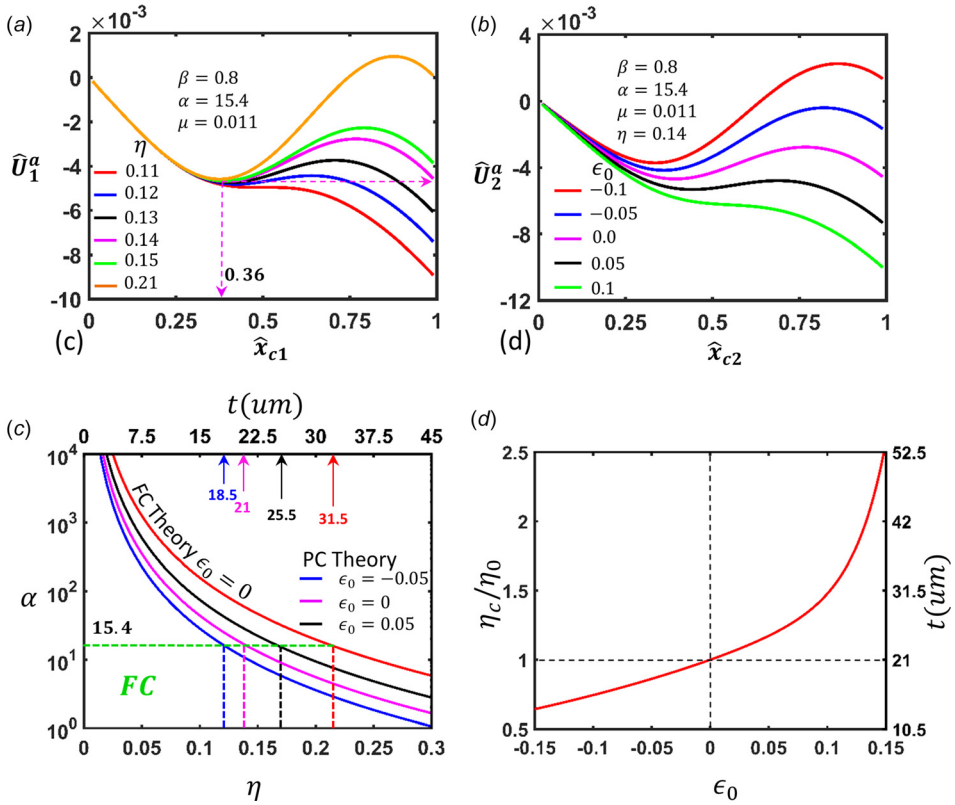

Fig. 3 (*a*) Normalized total energy of the system as a function of contact zone variable $\hat{x}_{c1}$ at state 1 of Fig. 2(*a*) with $\beta = 0.8, \alpha = 15.4$, and $\mu = 0.011$ fixed. Six different $\eta = 0.11, 0.12, 0.13, 0.14, 0.15$, and 0.21 are plotted where $\eta = 0.14$ (magenta curve) is the critical membrane thickness for FC. (*b*) Normalized total energy of the system as a function of contact zone variable $\hat{x}_{c2}$ at state 2 of Fig. 2(*a*) with $\beta = 0.8, \alpha = 15.4$, $\mu = 0.011$, and $\eta = 0.14$ fixed. Five different applied strains $\epsilon_0 = -0.1, -0.05, 0, 0.05$, and 0.1 are plotted. (*c*) Critical combinations of η and α for FC according to the FC theory (red curve) and the PC theory (blue, magenta, and black) with $\beta = 0.8$ and $\mu = 0.011$ fixed. (*d*) Critical membrane thickness for FC as a function of applied strain ϵ_0 (The reader is referred to the web version of this paper for the color representation of this figure.)

(blue and black), there is an energy barrier before reaching $\hat{x}_{c1} = 1$. This indicates that PC mode, though excluded by FC theory, could be a locally stable state during the transition from NC to FC. When $\eta = \eta_0 = 0.14$ (magenta), i.e., $t_0 = 21$ μm, there are two global minimums, $\hat{x}_{c1} = 0.36$ and $\hat{x}_{c1} = 1$. Thus, $\eta_0 = 0.14$ is the critical thickness of membrane that assures FC based on the PC theory. For thicker membranes, e.g., $\eta = 0.15$ and 0.21 (green and brown), the global minimum falls at $\hat{x}_{c1} = 0.36$ and $\hat{x}_{c1} = 0.30$, respectively, which indicates that PC is preferred over FC. In summary, we discover that the critical thickness predicted by the PC theory ($t_0 = 21$ μm) is 33% smaller than that predicted by the FC theory (31.5 μm). This is because the FC theory dismisses the possibility of PC so that the minimal energy is searched only within FC and NC scenarios. In other words, the critical membrane thickness in the FC theory is obtained by equating the total energy at $\hat{x}_{c1} = 0$ and $\hat{x}_{c1} = 1$, which is the case for the brown curve in Fig. 3(*a*). Nevertheless, the PC theory claims that even when $\hat{U}_1^a|_{\text{FC}} < \hat{U}_1^a|_{\text{NC}}$ is satisfied, the FC may not be the most energetically favorable state because there may be a global energy minimum in between, e.g., at $\hat{x}_{c1} = 0.32$ when $\eta = 0.15$ (green).

3.2 Strained after Lamination. Due to the limitation of the FC theory, when discussing the conformability after straining, we only focus on the results of the PC theory. First, by fixing $\eta = \eta_0 = 0.14$, i.e., critical thickness $t_0 = 21$ μm of the membrane, we can investigate how the stretching and compression of the substrate affect the conformability. Figure 3(*b*) presents the normalized total energy at State 2 as a function of $\hat{x}_{c2}$ with $\epsilon_0 = -0.1, -0.05, 0, 0.05$ and 0.1. It clearly shows that when stretching is applied, e.g., when $\epsilon_0 = 0.05$ and 0.1 (black and green), the right part of the energy curve bends down, thus FC can be maintained. However, when compression is applied, e.g., when $\epsilon_0 = -0.05$ and -0.1 (blue and red), the right part of the energy curve bends up and global minimum shifts to the middle, hence FC will change to PC under compression. The discovery that conformability can improve when stretching is applied can be easily explained using loading path (b). In fact, stretching the substrate in state 1 effectively reduces the surface roughness of the substrate.

One application of this result is illustrated in Fig. 3(*c*), which plots the critical (η, α) combination left to or below which FC can be achieved. The red curve in Fig. 3(*c*) represents the FC criterion given by the FC theory when $\epsilon_0 = 0$, i.e., Eq. (9). When $\alpha = 15.4$, as used in the previous example, the intersection between the dashed green line and the red curve gives the critical thickness of the membrane, which is $\eta = 0.21$ or $t = 31.5$ μm as pointed by the red arrow close to the upper horizontal axis. The magenta curve plots the critical (η, α) combination based on the PC theory when $\epsilon_0 = 0$, i.e., Eq. (27). When $\alpha = 15.4$, the critical thickness is $\eta_0 = 0.14 \text{or} t = 21 \mu\text{m}$. When a tensile strain, $\epsilon_0 = 0.05$, is applied, the result shifts right to be the black curve, such that the critical thickness enlarges to $t = 25.5$ μm. When a compressive strain, $\epsilon_0 = -0.05$, is applied, the magenta curve shifts left to be the blue curve, such that the critical thickness reduces to $t = 18.5$

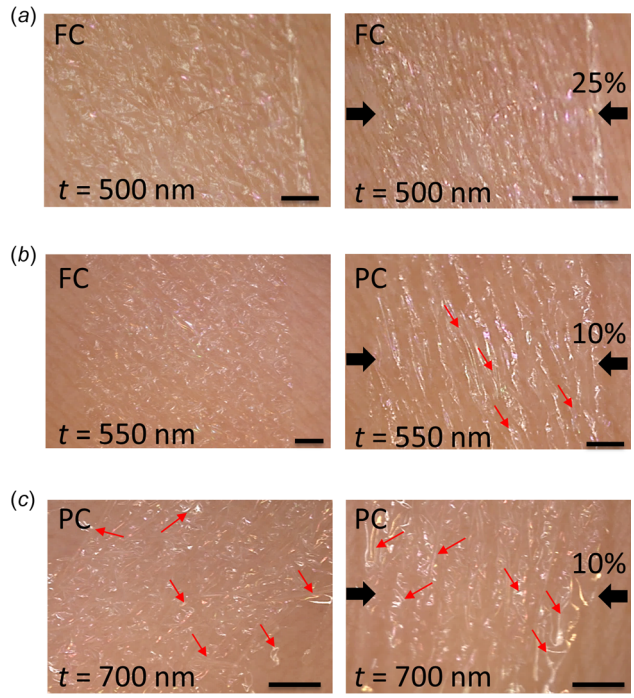

Fig. 4 Experimental pictures of PMMA membranes on human skin: (*a*) membrane of thickness $t = 500$ nm can fully conform to the skin with or without skin compression, (*b*) membrane of thickness $t = 550$ nm fully conforms to relaxed skin but experiences partial delamination under a compression of 10%, and (*c*) membrane of thickness $t = 700$ nm cannot form FC even with relaxed skin and more delaminations appear after a compression of 10%. Scale bar indicates 1 mm.

μm. Therefore, when a substrate is subjected to arbitrary lateral strain between $-0.05 < \epsilon_0 < 0.05$, it is easy to conclude that the critical thickness for the membrane to always stay FC should be $t = 18.5$ μm.

We may directly visualize the critical thickness η_c as a function of ϵ_0 in Fig. 3(*d*). We normalize η_c by $\eta_0 = 0.14$, which is the critical thickness at $\epsilon_0 = 0$ obtained by the PC theory. The actual thickness is denoted by the vertical axis on the right. It is manifest that the critical thickness monotonically increases with increasing ϵ_0, which has an opposite trend to that reported in Refs. [17,23] due to the inversed sign before ϵ_0 in their substrate energy equations as pointed out before. The prediction that stretching allows for thicker membrane to conform can be comprehended by imagining an extreme case in which very large stretching is applied. In this case, the rough surface of the substrate would flatten to an almost smooth surface and then membrane of any thickness would be able to fully conform to it. The other difference is that our plot is based on the PC theory but plots in Refs. [17,23] were based on the FC theory.

3.3 Predicting Critical Strain to Losing FC. Another application of our PC theory is to predict the change of conformability with different applied strain. The loading has to be quasi-static as the theory does not involve dynamics analysis. Recently, Ameri et al. [30,31] have fabricated an ultrathin and transparent graphene electronic tattoo (GET) sensor that is imperceptible on human skin but can perform multimodal vital sign monitoring. The graphene layer is supported by a transparent PMMA substrate which provides necessary mechanical support for processing and also for transferring GET to human skin. Since graphene thickness is much less compared with the PMMA, the thickness and mechanical properties of the GET are dominated by the PMMA. To fully understand GET conformability on human skin, here we conducted a series of experiments using blanket PMMA membranes with thicknesses of 500 nm, 550 nm, and 700 nm, and we observed three different conforming behaviors within such a small thickness range. Figure 4 displays multiple experimental pictures of those PMMA membranes on human skin with and without skin deformation. It is interesting to note that 500 nm thick PMMA can fully conform to the skin upon lamination and can stay conformed even under 25% compression (Fig. 4(*a*)). In contrast, Fig. 4(*b*) shows that 550 nm thick PMMA can fully conform to the relaxed skin but when subjected to 10% compression, internal delaminations can be observed, as indicated by small red arrows. When PMMA is 700 nm thick, Fig. 4(*c*) clearly suggests that it cannot even conform to relaxed skin. With a compression of 10%, more delamination occurred.

We now can use our PC theory to understand previously mentioned experimental observations. Parameters are chosen to be $h_0 \approx 20$ μm, $\lambda_0 \approx 150$ μm [27], $\bar{E}_s \approx 130$ kPa [28], $\bar{E}_m \approx 3.3$ GPa [30,31], and $\gamma \approx 18$ mJ/m^2 [32]. Accordingly, the

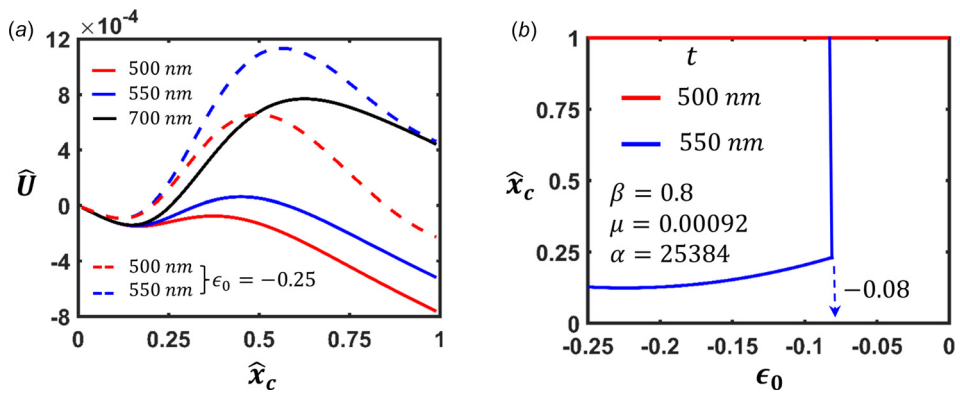

Fig. 5 Analytical prediction of conformability of PMMA membrane. (*a*) Normalized total energy of the system as a function of contact zone variable $\hat{x}_c$ with $\beta = 0.8, \alpha = 25384$, and $\mu = 0.00092$ fixed. At state 1, three thicknesses of PMMA $t = 500, 550$, and 700 nm are plotted as solid curves; at state 2 (e.g., $\epsilon_0 = -0.25$), $t = 500$, and 550 nm are plotted as dashed curves. (*b*) Conformability as a function of ϵ_0 for PMMAs of thicknesses $t = 500$ nm (red) and 550 nm (blue). Snap-through transition from FC to PC is predicted at $\epsilon_0 = -0.08$ when $t = 550$ nm while PMMA with $t = 500$ nm remains FC throughout the compression up to $\epsilon_0 = -0.25$ (The reader is referred to the web version of this paper for the color representation of this figure.)

nondimensional parameters can be calculated as $\beta = 2\pi h_0/\lambda_0 = 0.8$, $\alpha = \overline{E}_m/\overline{E}_s = 25384$, and $\mu = \gamma/(\overline{E}_s\lambda_0) = 0.00092$. Plugging into Eq. (24), the system energy after lamination (solid curves) and after compression (dashed curves) for different $t = 500, 550$, and 700 nm are shown in Fig. 5(*a*). It is obvious that the minimal total energy of 500 nm (red solid curve) and 550 nm thick PMMA (blue solid curve) after skin lamination falls at $\widehat{x}_c = 1$ (FC) while that of 700 nm thickness (black curve) falls at $\widehat{x}_c = 0.21$ (PC). This is fully consistent with our experimental observations in the left column of Fig. 4, i.e., 500 nm and 550 nm thick PMMA can fully conform to relaxed skin while 700 nm thick one cannot. When $\epsilon_0 = -0.25$ is applied, the solid red curve shifts to the dashed red curve, whose global minimum still locates at $\widehat{x}_c = 1$, which explains why the 500 nm thick PMMA remained FC under 25% skin compression (Fig. 4(*a*)). In contrast, for 550 nm thick PMMA, the blue solid curve is bent to the blue dashed curve after $\epsilon_0 = -0.25$, in which case the total minimal energy changes from $\widehat{x}_c = 1$ to $\widehat{x}_c = 0.17$, i.e., the conformability status switches from FC to PC (Fig. 4(*b*)). The relationship between $\widehat{x}_c$ and ϵ_0 is plotted in Fig. 5(*b*). As expected, the 500 nm thick PMMA (red curve) can stay FC up to 25% skin compression whereas the conformability of the 550 nm thick PMMA (blue curve) suddenly drops from FC to PC upon compression at $\epsilon_0 = -0.08$, which explains why we see delamination at 10% compression in our experiment (Fig. 4(*b*)). It is worth noting that this snap-through transition is similar to those reported in previous works [18,33,34]. After the sudden change from FC to PC at $\epsilon_0 = -0.08$, our PC theory can continue to predict the change of contact area upon further compression. It is surprising that when the thickness only drops by 50 nm, the 500 nm PMMA (red curve) survives compressive strain of 0.25, which makes it a very good choice for GET because it well balances the tradeoff between conformability and thickness (robustness). However, we have to admit that our current theory is developed within the scope of linear elasticity; hence, the predictions for strains beyond 10% will not be very accurate.

4 Conclusion

Using the method of energy minimization, this paper develops a theoretical framework to determine the conformability of a thin elastic membrane placed on a soft substrate with slightly wavy surface subjected to stretching/compression. By proving that the laminate-stretching and stretch-laminating loading paths can lead to exactly the same final states for the fully conformed scenario, we demonstrate that the stretch-laminating loading path can also be employed to solve partial conformability under linear elasticity assumptions. Our theory suggests that stretching improves the conformability while compression impairs it, which can be explained by the fact that stretching actually reduces the roughness of the substrate. Furthermore, this framework provides a viable method to predict the conformability and the contact area when the substrate has lateral strain. The critical membrane thickness and membrane-to-substrate stiffness ratio are quantitatively identified for full conformability. Our theory can also be used to predict the strain at which full conformability can no longer sustain. Our theory has been validated by laminating PMMA membranes of different thicknesses on human skin and inducing skin deformation.

Acknowledgment

L.W. acknowledges the CSE Harry Philip Whitworth Endowed Graduate Fellowship of the Cockrell School of Engineering.

Funding Data

- National Science Foundation (Grant No. 1663551).
- Office of Naval Research (Grant No. N00014-16-2044).

Appendix

A.1 Substrate Energy at State 2, i.e., U^a_{s2} in FC

According to the linear perturbation analysis in Ref. [25], the displacement field at state 2 in loading path (a) is given

$$u_x = \epsilon_0 x + \frac{h_0}{2(1-\nu)} e^{k\omega} \times \sin kx \left[(1-2\nu+k\omega)\frac{h_2-h_0}{h_0} - (3-2\nu+k\omega)\epsilon_0 \right]$$
$$u_y = -\frac{\nu}{1-\nu}\epsilon_0\omega + \frac{h_0}{2(1-\nu)} \times \cos kx \left\{ -2\nu\epsilon_0 + e^{k\omega}\left[(2-2\nu-k\omega)\frac{h_2-h_0}{h_0} + (2\nu+k\omega)\epsilon_0 \right] \right\} \tag{A1}$$

where $k = 2\pi/\lambda$, ν is the Poisson's ratio of the substrate, and $\omega = y - h_0\cos(kx)$ which transforms the substrate with sinusoidal surface to a semi-infinite solid with flat surface $(-\infty < x < \infty, -\infty < \omega < 0)$. The stress and strain fields can be derived accordingly and integrating $(1/2)\sigma_{ij}\epsilon_{ij}$ over the entire substrate gives the substrate energy at state 2 in Fig. 1(*a*)

$$U^a_{s2} = \frac{\pi}{4\lambda_2}\overline{E}_s\left[(h_2-h_0)^2 + 2h_0(h_2-h_0)\epsilon_0\right] + \frac{\overline{E}_s\epsilon_0^2}{2}H_{\text{sub}} \tag{A2}$$

where H_{sub} is the thickness of the substrate and $H_{\text{sub}} \to \infty$ is assumed throughout our analysis. The second term is a constant $C \equiv 1/2\overline{E}_s\epsilon_0^2 H_{\text{sub}}$. Note that the substrate energy given in Refs. [17,23] has an inverse sign in front of the ϵ_0 term, which leads to a trend opposite to Fig. 3(*d*).

A.2 Substrate Energy at State 1, i.e., U^b_{s1} in FC

According to the linear perturbation analysis in Ref. [25], the displacement field at state 1 in loading path (b) is given by

$$u_x = \epsilon_0 x + (\epsilon_0 h_0)\left(\frac{-2+2\nu-k\omega}{1-\nu}e^{k\omega}\sin kx\right)$$
$$u_y = -\frac{\nu}{1-\nu}\epsilon_0\omega + (\epsilon_0 h_0)\left[\left(\frac{-2+2\nu+k\omega}{1-\nu}e^{k\omega} - \frac{\nu}{1-\nu}\right)\cos kx + 1\right] \tag{A3}$$

The stress–strain fields can be obtained out of the displacement field and integrating $(1/2)\sigma_{ij}\epsilon_{ij}$ over the substrate domain gives the substrate energy per wavelength

$$U^b_{s1} = \frac{\overline{E}_s\epsilon_0^2}{2}H_{\text{sub}} + \frac{\overline{E}_s\pi h_0^2\epsilon_0^2(5-20\nu+16\nu^2)}{8\lambda_0(1-\nu)(2\nu-1)} \approx \frac{\overline{E}_s\epsilon_0^2}{2}H_{\text{sub}} \equiv C \tag{A4}$$

The first term is simply equal to the work done by the external load on a semi-infinite elastic body with thickness of H_{sub}. The second term is omitted as $H_{\text{sub}} \gg h$. Therefore, U^b_{s1} is independent of H_2; thus, it does not play a role in the variation of the total energy.

A.3 Substrate Energy at State 1, i.e., U^a_{s1} in PC

The substrate energy is given in Ref. [18]

$$U^a_{s1} = \frac{\overline{E}_s\lambda_1\beta^2(1-\xi)^2}{4\pi}F(\widehat{x}_{c1}) \tag{A5}$$

$F(\widehat{x}_{c1})$ can be analytically solved as follows:

$$F(\hat{x}_{c1}) = \frac{1}{\lambda_1}\int_0^{x_{c1}} \left\{ 2\left(1+\cos\frac{2\pi x}{\lambda_1}\right)\cos\frac{\pi x}{\lambda_1}\sqrt{\left(\sin\frac{\pi x_{c1}}{\lambda_1}\right)^2 - \left(\sin\frac{\pi x}{\lambda_1}\right)^2} - \left(1+\cos\frac{2\pi x}{\lambda_1}\right)\left(\sin\frac{\pi x_{c1}}{\lambda_1}\right)^2 \right.$$
$$\left. \times \cos\frac{\pi x}{\lambda_1}\left[\sqrt{\left(\cos\frac{\pi x}{\lambda_1}\right)^2 - \left(\cos\frac{\pi x_{c1}}{\lambda_1}\right)^2}\right]^{-1} \right\} dx = \frac{1}{4}\sin^4\left(\frac{\pi x_{c1}}{\lambda_1}\right) = \frac{1}{4}\sin^4\left(\frac{\pi \hat{x}_{c1}}{2}\right) \tag{A6}$$

References

[1] Kim, D.-H., Ghaffari, R., Lu, N., and Rogers, J. A., 2012, "Flexible and Stretchable Electronics for Biointegrated Devices," Annu. Rev. Biomed. Eng., **14**, pp. 113–128.

[2] Lu, N., and Kim, D.-H., 2014, "Flexible and Stretchable Electronics Paving the Way for Soft Robotics," Soft Rob., **1**(1), pp. 53–62.

[3] Rogers, J. A., Someya, T., and Huang, Y. G., 2010, "Materials and Mechanics for Stretchable Electronics," Science, **327**(5973), pp. 1603–1607.

[4] Lu, N. S., and Yang, S. X., 2015, "Mechanics for Stretchable Sensors," Curr. Opin. Solid State Mater. Sci., **19**(3), pp. 149–159.

[5] Suo, Z. G., 2012, "Mechanics of Stretchable Electronics and Soft Machines," MRS Bull., **37**(3), pp. 218–225.

[6] Forrest, S. R., 2004, "The Path to Ubiquitous and Low-Cost Organic Electronic Appliances on Plastic," Nature, **428**(6986), pp. 911–918.

[7] Oh, J. Y., Rondeau-Gagne, S., Chiu, Y. C., Chortos, A., Lissel, F., Wang, G. J. N., Schroeder, B. C., Kurosawa, T., Lopez, J., Katsumata, T., Xu, J., Zhu, C. X., Gu, X. D., Bae, W. G., Kim, Y., Jin, L. H., Chung, J. W., Tok, J. B. H., and Bao, Z. N., 2016, "Intrinsically Stretchable and Healable Semiconducting Polymer for Organic Transistors," Nature, **539**(7629), pp. 411–415.

[8] Akinwande, D., Petrone, N., and Hone, J., 2014, "Two-Dimensional Flexible Nanoelectronics," Nat. Commun., **5**, p. 5678.

[9] Carlson, A., Bowen, A. M., Huang, Y. G., Nuzzo, R. G., and Rogers, J. A., 2012, "Transfer Printing Techniques for Materials Assembly and Micro/Nanodevice Fabrication," Adv. Mater., **24**(39), pp. 5284–5318.

[10] Yang, S., Chen, Y. C., Nicolini, L., Pasupathy, P., Sacks, J., Becky, S., Yang, R., Daniel, S., Chang, Y. F., Wang, P., Schnyer, D., Neikirk, D., and Lu, N., 2015, " 'Cut-and-Paste' Manufacture of Multiparametric Epidermal Sensor Systems," Adv. Mater., **27**(41), pp. 6423–6430.

[11] Fukuda, K., and Someya, T., 2017, "Recent Progress in the Development of Printed Thin-Film Transistors and Circuits With High-Resolution Printing Technology," Adv. Mater., **29**(25), p. 1602736.

[12] Kim, D. H., Lu, N. S., Ma, R., Kim, Y. S., Kim, R. H., Wang, S. D., Wu, J., Won, S. M., Tao, H., Islam, A., Yu, K. J., Kim, T. I., Chowdhury, R., Ying, M., Xu, L. Z., Li, M., Chung, H. J., Keum, H., McCormick, M., Liu, P., Zhang, Y. W., Omenetto, F. G., Huang, Y. G., Coleman, T., and Rogers, J. A., 2011, "Epidermal Electronics," Science, **333**(6044), pp. 838–843.

[13] Hammock, M. L., Chortos, A., Tee, B. C. K., Tok, J. B. H., and Bao, Z. A., 2013, "25th Anniversary Article: The Evolution of Electronic Skin (E-Skin): A Brief History, Design Considerations, and Recent Progress," Adv. Mater., **25**(42), pp. 5997–6037.

[14] Park, S. I., Brenner, D. S., Shin, G., Morgan, C. D., Copits, B. A., Chung, H. U., Pullen, M. Y., Noh, K. N., Davidson, S., and Oh, S. J., 2015, "Soft, Stretchable, Fully Implantable Miniaturized Optoelectronic Systems for Wireless Optogenetics," Nat. Biotechnol., **33**(12), p. 1280.

[15] Wang, S. D., Li, M., Wu, J., Kim, D. H., Lu, N. S., Su, Y. W., Kang, Z., Huang, Y. G., and Rogers, J. A., 2012, "Mechanics of Epidermal Electronics," ASME J. Appl. Mech., **79**(3), p. 031022.

[16] Jeong, J.-W., Yeo, W.-H., Akhtar, A., Norton, J. J. S., Kwack, Y.-J., Li, S., Jung, S.-Y., Su, Y., Lee, W., Xia, J., Cheng, H., Huang, Y., Choi, W.-S., Bretl, T., and Rogers, J. A., 2013, "Materials and Optimized Designs for Human-Machine Interfaces Via Epidermal Electronics," Adv. Mater., **25**(47), pp. 6839–6846.

[17] Cheng, H., and Wang, S., 2013, "Mechanics of Interfacial Delamination in Epidermal Electronics Systems," ASME J. Appl. Mech., **81**(4), p. 044501.

[18] Wang, L., and Lu, N., 2016, "Conformability of a Thin Elastic Membrane Laminated on a Soft Substrate With Slightly Wavy Surface," ASME J. Appl. Mech., **83**(4), p. 041007.

[19] Kim, D.-H., Viventi, J., Amsden, J. J., Xiao, J., Vigeland, L., Kim, Y.-S., Blanco, J. A., Panilaitis, B., Frechette, E. S., Contreras, D., Kaplan, D. L., Omenetto, F. G., Huang, Y., Hwang, K.-C., Zakin, M. R., Litt, B., and Rogers, J. A., 2010, "Dissolvable Films of Silk Fibroin for Ultrathin Conformal Bio-Integrated Electronics," Nat. Mater., **9**(6), pp. 511–517.

[20] Xu, L., Gutbrod, S. R., Bonifas, A. P., Su, Y., Sulkin, M. S., Lu, N., Chung, H.-J., Jang, K.-I., Liu, Z., Ying, M., Lu, C., Webb, R. C., Kim, J.-S., Laughner, J. I., Cheng, H., Liu, Y., Ameen, A., Jeong, J.-W., Kim, G.-T., Huang, Y., Efimov, I. R., and Rogers, J. A., 2014, "3D Multifunctional Integumentary Membranes for Spatiotemporal Cardiac Measurements and Stimulation Across the Entire Epicardium," Nat. Commun., **5**, p. 3329.

[21] Kim, D.-H., Ghaffari, R., Lu, N., Wang, S., Lee, S. P., Keum, H., D'Angelo, R., Klinker, L., Su, Y., and Lu, C., 2012, "Electronic Sensor and Actuator Webs for Large-Area Complex Geometry Cardiac Mapping and Therapy," Proc. Natl. Acad. Sci., **109**(49), pp. 19910–19915.

[22] Jeong, J. W., Kim, M. K., Cheng, H., Yeo, W. H., Huang, X., Liu, Y., Zhang, Y., Huang, Y., and Rogers, J. A., 2014, "Epidermal Electronics: Capacitive Epidermal Electronics for Electrically Safe, Long-Term Electrophysiological Measurements," Adv. Healthcare Mater., **3**(5), p. 621.

[23] Dong, W., Xiao, L., Zhu, C., Ye, D., Wang, S., Huang, Y., and Yin, Z., 2017, "Theoretical and Experimental Study of 2D Conformability of Stretchable Electronics Laminated Onto Skin," Sci. China Technol. Sci., **60**, pp. 1–8.

[24] Xiao, J., Carlson, A., Liu, Z., Huang, Y., Jiang, H., and Rogers, J., 2008, "Stretchable and Compressible Thin Films of Stiff Materials on Compliant Wavy Substrates," Appl. Phys. Lett., **93**(1), p. 013109.

[25] Xiao, J., Carlson, A., Liu, Z. J., Huang, Y., and Rogers, J. A., 2010, "Analytical and Experimental Studies of the Mechanics of Deformation in a Solid With a Wavy Surface Profile," ASME J. Appl. Mech., **77**(1), p. 011003.

[26] Huang, Z. Y., Hong, W., and Suo, Z., 2005, "Nonlinear Analyses of Wrinkles in a Film Bonded to a Compliant Substrate," J. Mech. Phys. Solids, **53**(9), pp. 2101–2118.

[27] Tchvialeva, L., Zeng, H., Markhvida, I., McLean, D. I., Lui, H., and Lee, T. K., 2010, "Skin Roughness Assessment," *New Developments in Biomedical Engineering*, D. Campolo, ed., InTech, Rijeka, Croatia, pp. 341–358.

[28] Pailler-Mattei, C., Bec, S., and Zahouani, H., 2008, "In Vivo Measurements of the Elastic Mechanical Properties of Human Skin by Indentation Tests," Med. Eng. Phys., **30**(5), pp. 599–606.

[29] Meitl, M. A., Zhu, Z.-T., Kumar, V., Lee, K. J., Feng, X., Huang, Y. Y., Adesida, I., Nuzzo, R. G., and Rogers, J. A., 2006, "Transfer Printing by Kinetic Control of Adhesion to an Elastomeric Stamp," Nat. Mater., **5**(1), pp. 33–38.

[30] Ameri, S., Ho, R., Jang, H., Wang, Y., Schnyer, D., Akinwande, D., and Lu, N., 2016, "Thinnest Transparent Epidermal Sensor System Based on Graphene," IEEE International Electron Devices Meeting (IEDM), San Francisco, CA, Dec. 3–7.

[31] Kabiri Ameri, S., Ho, R., Jang, H., Tao, L., Wang, Y., Wang, L., Schnyer, D. M., Akinwande, D., and Lu, N., 2017, "Graphene Electronic Tattoo Sensors," ACS Nano, **11**(8), pp. 7634–7641.

[32] Brennan, C. J., Nguyen, J., Yu, E. T., and Lu, N., 2015, "Interface Adhesion Between 2D Materials and Elastomers Measured by Buckle Delaminations," Adv. Mater. Interfaces, **2**(16), p. 1500176.

[33] Wagner, T. J., and Vella, D., 2012, "The Sensitivity of Graphene "Snap-Through" to Substrate Geometry," Appl. Phys. Lett., **100**(23), p. 233111.

[34] Qiao, S. T., Gratadour, J. B., Wang, L., and Lu, N. S., 2015, "Conformability of a Thin Elastic Membrane Laminated on a Rigid Substrate With Corrugated Surface," IEEE Trans. Compon., Packag., Manuf. Technol., **5**(9), pp. 1237–1243.